The Art of Modelling Stars in the 21st Century
Proceedings IAU Symposium No. 252, 2008
L. Deng & K.L. Chan, eds.

doi:10.1017/S1743921308022722

Hydrodynamical Simulations of Turbulent Convection in a Rotating Red Giant Star

A. Palacios[1,2] and A. S. Brun[2]

[1]Université Montpellier II – GRAAL, CNRS – UMR 5024, place Eugène Bataillon, F-34095 Montpellier, France
email: palacios@graal.univ-montp2.fr

[2]CEA/DSM/IRFU/SAp – L'Orme des Merisiers bât 709 – F-91191 Gif-sur-Yvette (France)
email: asbrun@cea.fr

Abstract. We present 3-D hydrodynamical simulations of the extended turbulent convective envelope of a low-mass red giant star. These simulations, computed with the ASH code, aim at understanding the redistribution of angular momentum and heat in extended turbulent convection zones of these giant stars. We focus our study on the effects of turbulence and of the rotation rate on the convective patterns and on the distribution of angular momentum within the inner 50% of the convective envelope of such stars.

Keywords. Hydrodynamics, convection, stars: rotation, stars: evolution

1. Introduction

Turbulent convection is still poorly known and understood in the extended envelopes of giant stars, and its interaction with rotation also needs to be more deeply understood. As of today, our understanding of stellar evolution is based on 1-D stellar evolution codes that compute the late evolution of stars on the giant branch by assuming mixing length theory (Bohm-Vitense 1958). The mixing length parameter α used for red giant models is generally calibrated on the main sequence so as to fit the Sun (Brun *et al.* 2002). In more sophisticated rotating evolutionary models, the transport of angular momentum in radiative regions is ensured by meridional circulation and shear-induced turbulence (Zahn 1992), while solid-body rotation is assumed in convective regions (e.g. strong turbulent diffusion of the angular momentum) in the absence of a reliable formalism to describe the transport of angular momentum in these regions. These assumptions, both on the mixing length parameter and on the angular momentum distribution inside convective regions are based on simple arguments developed many decades ago to model the Sun (and even for our closest star this does not necessarily hold true today, Brun & Toomre 2002, Miesch *et al.* 2008). Further the structure and the properties of the convective envelope of red giant stars are completely different from that of the Sun. The combination of determinations of $v \sin i$ for stars in different evolutionary phases indicates that the assumption of solid-body rotation in extended low-density convective envelopes is most likely erroneous. In particular, the analysis of the rotation of horizontal branch stars in globular clusters led Sills & Pinsonneault (2000) to suggest that in order to reproduce the rotation velocity of HB stars considering that the progenitors of these stars on the red giant branch had almost zero surface rotation, a large amount of angular momentum should be retained in the inner part of the stars during the RGB ascension. This can be achieved if RGB convective envelopes rotate differentially. In the following work, we investigate more deeply the interaction of turbulent convection and rotation in such an extended convective zone using 3-D simulations in an attempt to address these important

scientific topics. In section 2 we briefly discuss the numerical model, in §3 the patterns realized in the convective envelope, in §4 the angular momentum redistribution within the shell and conclude in §5.

2. Physical Inputs and Numerical Simulations with the ASH code

We have used the Anelastic Spherical Harmonic (ASH) code in its purely hydrodynamic mode to study the convection in extended envelope of a low-mass red giant (RGB) star (Palacios & Brun 2007). The ASH code has been successfully applied to study convection in different types of stars such as the Sun or massive stars (Brun & Toomre 2002, Miesch *et al.* 2006, Browning *et al.* 2004). These recent successes give credit to the present simulations. The reader is referred to Brun *et al.* (2004) for details on the code. Let us here briefly summarize the main characteristics of our simulations. To build the 3-D nonlinear simulation we used a 1-D red giant stellar model as initial state, whose characteristics are: $M_{\rm ini} = 0.8\ M_\odot$, $L_* = 425\ L_\odot$ and $R_* = 39\ R_\odot$. In order use a density contrast that can be numerically handled by ASH at a reasonable computational cost (e.g. $\rho_{\rm bottom}/\rho_{\rm top} = 100$), we only consider the inner 50% of the convective envelope, e.g. $r \in [0.05\ R_*; 0.5\ R_*]$. This choice is also driven by the fact that getting too close to the surface would imply large Mach numbers that are not compatible with the anelastic assumption. We assume that the convective envelope initially rotates as a solid-body, and we adopt two different initial rotation rates : a tenth solar (case A), corresponding to $\upsilon_{eq,surf} \simeq 7$ km/s and a fiftieth solar (case B) corresponding to $\upsilon_{eq,surf} \simeq 1.4$ km/s. We assume rigid stress free boundary conditions at the edges of the computational domain, and impose a flux of radiative energy at the base of our domain that is extracted at the surface. The model parameters for cases A and B are given in Table 1.

Table 1. The Prandtl number is defined by ν_{top}/κ_{top}. The Rayleigh number $R_a = (-\partial\tilde{\rho}/\partial\tilde{S})\Delta S g L^3/\rho\nu\kappa$ (with ΔS the entropy contrast across the domain) is evaluated at mid-layer depth. The rms Reynolds number is given by $\tilde{R}_e = \tilde{v}L/\nu$, where $\tilde{v}$ is a representative rms convective velocity. In both cases $L = 1.22 \times 10^{22}$ cm. Time averages over the full computational domain of the total kinetic energy (KE), and that associated with the (axisymmetric) differential rotation (DRKE), the (axisymmetric) meridional circulation (MCKE) and the non-axisymmetric convection itself (CKE), all in units of ergs.cm^{-3}.

Simulation Parameters

Case	$\Omega_0/\Omega_\odot$	$N_r,\ N_\theta,\ N_\phi$	P_{rot}	ν_{top}	κ_{top}	P_r	R_e	R_a
A	0.1	256, 256, 512	273 d ($\times$ 12)	1.2×10^{15}	1.2×10^{15}	1	400	7.5×10^5
B	0.02	256, 256, 512	1398 d ($\times$ 6)	1.2×10^{15}	1.2×10^{15}	1	375	4.5×10^5

Time and Volume Averaged Energy Densities

	KE	DRKE	CKE	MCKE
A	1.36×10^6	4.69×10^5 (34.4 %)	7.86×10^5 (57.7 %)	1.07×10^5 (7.9 %)
B	2.18×10^6	1.36×10^5 (6.2 %)	1.80×10^6 (82.4 %)	2.47×10^5 (11.4 %)

3. Convective patterns

In both cases, the convective instability sets in during the first hundred days of the simulation and then undergoes non-linear saturation. It subsequently reaches a statistical

https://doi.org/10.1017/S1743921308022722 Published online by Cambridge University Press

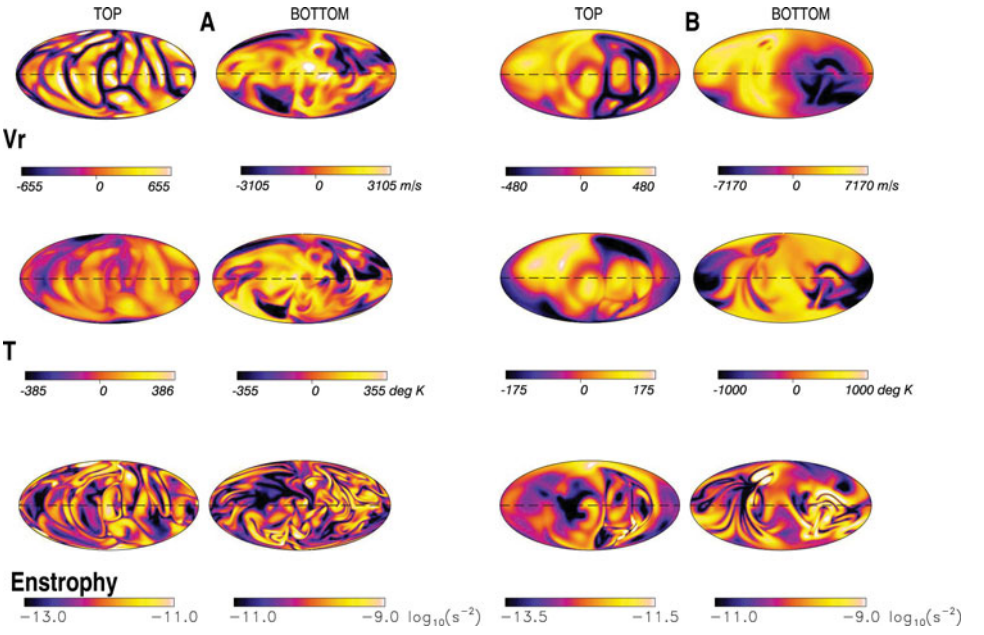

Figure 1. Convective patterns represented by the radial velocity V_r (first row) and the temperature T (second row) variations at the top and bottom edges of the computational domain for cases A (first two columns) and B (last two columns).

equilibrium that is maintained over the later evolution of the simulation. The simulations are thus considered to be relaxed (even though the model is still marginally evolving toward complete thermal equilibrium). The convective patterns that develop are shown in Fig. 1 after respectively 12 and 6 rotation periods of overall evolution for cases A and B respectively. Two different depths are shown : near the top (19 $R_\odot$), and at the bottom (3 $R_\odot$) of the computational domain.

The turbulent convection achieved in these simulations is characterized by large warm up-flows surrounded by cool narrower downflows at the top edge of the computational domain. For case A, the convective pattern consists of small number of cells uniformly distributed over the sphere, this pattern being toned down at larger depths. For case B, which rotates slowlier than case A, the number of cells is considerably reduced, and convection is strongly bipolar, with a warm and a cool side that are clearly distinct. This pattern resembles that obtained in non-rotating simulations (Woodward *et al.* 2003, Kuhlen *et al.* 2006), where the $\ell = 1$ mode is predicted to be dominant (case of incompressible fluid sphere at low R_a numbers, Chandrasekhar 1961).

In both cases, the strong correlation between radial velocity and temperature variations appearing in the maps results in an outward transport of heat. In order to actually transport the large luminosity of the star ($L \sim 400 L_\odot$), the velocity and temperature fluctuations are very large, up to 3000 m.s^{-1} and 400 K in case A, 7000 m.s^{-1} and 1000 K in case B. These variations are at least one order of magnitude larger than those found in the simulations of the solar convective envelope, where the radial velocity and temperature fluctuations do not exceed a few 100 m.s^{-1} and 10 K respectively. The even larger fluctuations that appear in case B indicate the stabilizing role of rotation (when significant) that leads to a less vigorous convective flow.

The convective luminosity is found to be significantly larger than the star's luminosity, in the bulk of the domain for case A and at the bottom of the domain for case B. This is

https://doi.org/10.1017/S1743921308022722 Published online by Cambridge University Press

to compensate a negative kinetic energy luminosity that can represent up to 70% of the total luminosity in case A and up to 120% in case B. This negative kinetic energy flux results from the strong asymmetry between up-flows and downflows in the bulk of the domain. It is thus even stronger in case B where the bipolarity of convection is strongly marked. This is an important result that contradicts the assumption of the mixing length theory, that assumes that the total and convective luminosity are equal.

The convection is found to possess a significant amount of vorticity that mainly concentrates around the strongest downflows as illustrated in Fig. 1 by the enstrophy map. It is obvious that case A possesses a more intricate and small scale enstrophy field which is the direct consequence of its larger rotation rate. Table 1 also summarizes the energetics of the convection for cases A and B.

In the bulk of our simulations, the kinetic energy density (KE) is dominated by convection, and the meridional circulation contributes significantly to the total energy (about 10% in both cases). This is clearly different than for the solar case, where the contribution of meridional circulation to the averaged total KE is less than 1%. For case B, the energy associated with meridional circulation is larger than that associated with differential rotation. This is actually not the case during the whole simulation : an alternation between phases with MCKE > DRKE and with MCKE < DRKE of variable length is found. This affects the meridional circulation pattern achieved in that simulation. When MCKE < DRKE, which is always true for case A, the meridional circulation pattern consists of one poleward cell per hemisphere. For case A, this pattern, presented in panel (a) of Fig. 3, is very stable over the simulation, in particular, no inversions of the meridional circulation are observed, and the total number of cells is always two. For case B, this pattern changes when MCKE > DRKE, and turns into a unique cell crossing the equator, and being equatorward in the northern hemisphere. Associated with this circulation is a strong bipolar structure, found both in the temperature and radial velocity fluctuations. Note however that the slow rotation rate of case B leads to a reduced rotational constrain on the flow. Forming axisymmetric averages around the axis of rotation may, in this case, lead to large fluctuation in the resulting averaged quantity by the simple misalignment of the large scale flow with respect to that axis (i.e the meridional flow may drift in latitude and longitude making it difficult to project into the meridional plane). The typical amplitudes of these large-scale circulations varies between 100 and 700 $\mathrm{m.s}^{-1}$ for case A and between 600 and 1600 $\mathrm{m.s}^{-1}$, depending on the location in the computational domain. This is much larger than what is found in the Sun (about 20 $\mathrm{m.s}^{-1}$ at the solar surface). The turnover time for the meridional circulation in both cases is much longer that the typical convection turnover time (3.5 years vs. 150 days for case A).

4. Angular momentum redistribution in the shell

In this extended convective envelope, our choice of stress-free velocity boundaries ensures that no torque is applied to the system, and that angular momentum is conserved in the convective shell. In turbulent convection zones, the angular momentum is redistributed by various physical processes, which are in turn, viscous diffusion, Reynolds stresses, and mean large scale circulations. We may identify the contribution to the transport of angular momentum of each process by considering the mean radial ($\mathcal{F}_r$) and latitudinal ($\mathcal{F}_\theta$) angular momentum fluxes. The expressions of these fluxes are given in Brun & Toomre 2002. Figure 3 presents these integrated averaged fluxes along co-latitude and radius for case A and case B respectively. We may first note the good quality of the angular momentum balance characterized by the solid lines, that is very close to zero (e.g. no net flux) in both cases A and B when averaging over the entire length of the simulations.

https://doi.org/10.1017/S1743921308022722 Published online by Cambridge University Press

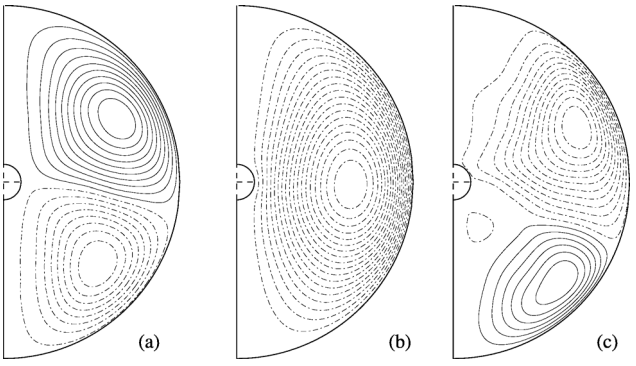

Figure 2. Streamlines of the meridional circulation currents. Dashed and solid lines indicate clockwise and counterclockwise circulation respectively. (a) corresponds to the mean pattern obtained in case A; (b) and (c) are associated with phases MCKE > DRKE and MCKE < DRKE respectively in case B.

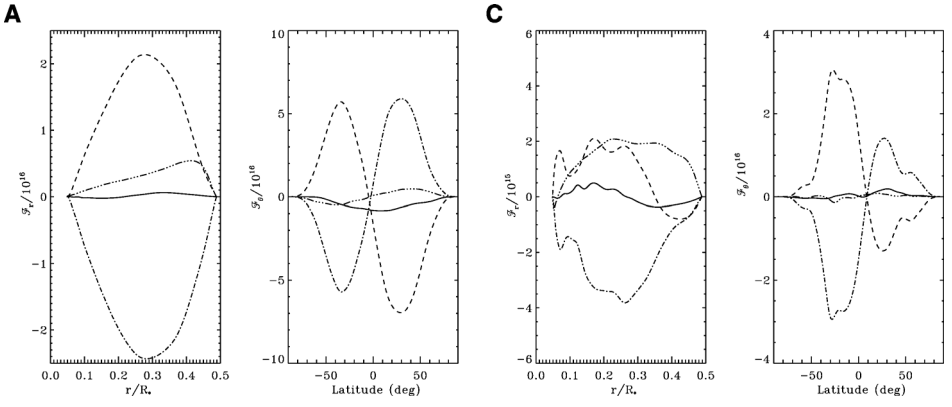

Figure 3. Time average of latitude line integral of the angular momentum flux $\mathcal{F}_r$ and of the radial line integral of the angular momentum $\mathcal{F}_\theta$ for cases A (left panels) and B(right panels). Viscous (dashed-triple-dotted), Reynolds stresses (dashed-dotted) and meridional circulation (dashed) contributions are represented together with the total fluxes (solid). Positive values indicate outward radial flux and northward latitudinal flux. Averages are over 12 and 6 rotation periods for cases A and B respectively.

In the latitudinal direction, the meridional circulation flux compensates that of the Reynolds stresses, with a poleward transport in the northern hemisphere for both cases A and B. The viscous transport is negligible. In the radial direction, the pictures differs in both cases. In the slowly rotating case (B) meridional circulation and Reynolds stresses are of opposite sign, but the viscous flux has the same amplitude and sign as meridional circulation flux, and plays an important role in the flux balance. As we will see in the forthcoming paragraph, this is associated with a shellular rotation achieved in this case. In the more rapidly rotating case (A), the balance in the radial directions resembles that in latitudinal direction: meridional circulation acts to transport the angular momentum outward, and is compensated by the Reynolds stresses (associated with $< v'_r v'_\phi >$). The viscous flux is negligible in this case.

The redistribution of angular momentum in the convective shell results in a strong departure from the initial solid-body rotation regime. The rotation achieved is substantially different according to the bulk angular velocity adopted as can be seen in Fig. 4.

https://doi.org/10.1017/S1743921308022722 Published online by Cambridge University Press

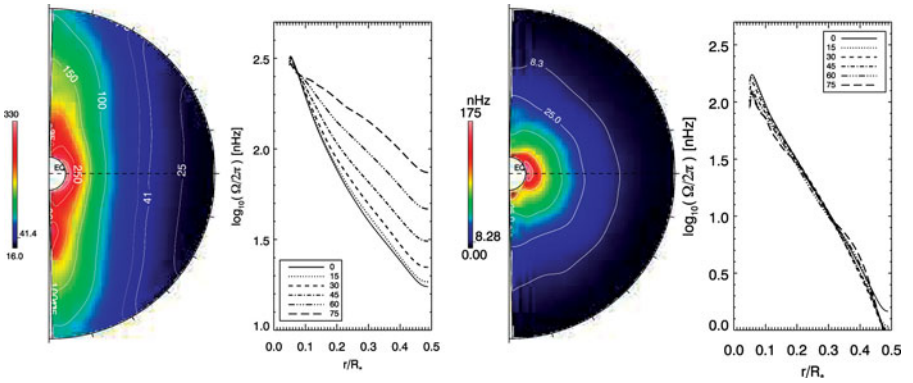

Figure 4. *2D plots* Temporal and longitudinal average of the angular velocity profile in cases A (left) and B (right). *1D plots* Radial profiles for selected latitudes (0,15,30,45,60,75 degrees) for cases A and B.

For case A, Ω_0 is larger than what would represent that of a real RGB star. A strong differential rotation is found in both radial and latitudinal directions ($\Delta\Omega/\Omega_0$ between 0° and 60° near the top of the domain close to 60%). The poles rotate faster than the equator (anti-solar rotation) and the inner and outer regions rotate in opposite directions. Ω contours are aligned with the rotation axis, resulting in an almost cylindrical pattern that might be attributed to the mild degree of turbulence of the simulation or to the absence of a strong latitudinal entropy contrast (Miesch *et al.* 2006).

For case B, which is more realistic compared to the actual rotation velocities determined in RGB stars, a strong shellular rotation is found : shells rotating as solid-bodies pile-up with increasing radial velocity towards the center. This leads to the large viscous transport found in the radial direction and to a more subtle balance of angular momentum (see §3). Independently of their latitudinal angular velocity profiles both models possess a strong radial differential rotation. This behaviour has also been reported by Steffen & Freytag (2007) in their rotating "star-in-a-box"experiments.

5. Conclusion

We have undertaken a series of hydrodynamical simulations of the turbulent convection in the rotating extended envelope of a RGB star, of which we have exposed here two cases with different bulk rotation rates.

The rotation rate appears to be crucial in determining both the convective pattern and the angular momentum redistribution. For more realistic values (case B) associated with $v_{eq,surf} \simeq 2$ km.s^{-1}, the convection is bipolar, as already observed in non-rotating simulations of the same kind. The enthalpy flux associated with the convection can be much larger that the total flux at the base of the domain, in order to compensate for the large negative kinetic fluxes. This is in contradiction with one of the basic assumptions of the mixing-length theory used in 1-D stellar evolution models to describe convection. The angular momentum redistribution leads to shellular rotation in the spherical shell, with a strong differential rotation in the radial direction. When rotation rate is increased (as in case A), the $\ell = 1$ mode does not dominate turbulent convection anymore, and the convective pattern becomes more complex. As in case B, the enthalpy flux again becomes larger that the total flux in the bulk of the domain, which confirms the contradiction with MLT. Concerning the redistribution of angular momentum, we observe the development and maintenance of a large cylindrical differential rotation within the inner part of the

https://doi.org/10.1017/S1743921308022722 Published online by Cambridge University Press

convective envelope of the RGB star. This regime contradicts the assumption of solid body rotation assumed in stellar evolution modeling. It could be of great importance for the global redistribution of angular momentum and chemical species in the underlying radiative region. We shall thus explore in more details the parameter space of our simulation in order to be able to propose a more realistic prescription for the angular momentum distribution within the convective envelope of red giant stars for 1-D stellar evolution.

Acknowledgement

The simulation has been carried out using the supercomputers of CEA-CCRT.

References

Bohm-Vitense, E. 1958, *Z. Astrophys.*, 54, 114
Browning, M. K., Brun, A. S., & Toomre, J. 2004, *ApJ*, 601, 512
Brun, A. S., Antia, H. M., Chitre, S. M., & Zahn, J.-P. 2002, *A&A*, 391, 725
Brun, A. S., Miesch, M. S., & Toomre, J. 2004, *ApJ*, 614, 1073
Brun, A. S., & Toomre, J. 2002, *ApJ*, 570, 865
Chandrasekhar, S. 1961, *Hydrodynamic and hydromagnetic stability - International Series of Monographs on Physics, Oxford: Clarendon*
Kuhlen, M., Woosley, S. E., & Glatzmaier, G. A. 2006, *ApJ*, 640, 407
Miesch, M. S., Brun, A. S., & Toomre, J. 2006, *ApJ* 641, 618
Miesch, M. S., Brun, A. S., Derosa, M., Toomre, J. 2008, *ApJ*, 673, 557
Palacios, A., & Brun, A. S., *Astronomical Notes*, 328, 1114
Palacios, A., Charbonnel, C., Talon, S., & Siess, L. 2006, *A&A* 453, 261
Sills, A., & Pinsonneault, M. 2000, *ApJ* 540, 489
Steffen, M. & Freytag, B, 2007, *Astronomical Notes*, 328, 1054
Sweigart, A. V. & Mengel, J. G. 1979, *ApJ* 229, 624
Woodward, P. R., Porter, D. H., & Jacobs, M. 2003, *3D Stellar Evolution*, 293, 45
Zahn, J.-P. 1992, *A&A* 265, 115

Discussion

Ludwig: Remark: I found it very encouraging to see that two codes (your ASH code, and COSBOLD by Freytag & Steffen) give so similar results for rotating giants, considering the very different numerical approaches which are taken in the modeling.

Palacios: Thank you.

Chan: (1) What flux did you use in the model? (2) What is the thermal relaxation time for that flux?

Palacios: (1) The flux used in the model comes from the 1D stellar evolution model, that is realistic as far as stellar parameters are concerned. (2) The simulations have not reached the thermal relaxation, but as we start from a realistic structure that is thermally relaxed, we assume that it is not so crucial for our purpose.

Meynet: (1) How would you translate your 3D results into a rule for 1D models? (2) Do you plan to study the effects of a magnetic field?

Palacios: (1) We first want to explain the parameters of the simulations, but it is already clear that we should avoid considering uniform angular velocity in the extended envelopes of giants ($\Omega(r) = cte$). The assumption of uniform specific angular momentum

($r^2\Omega \propto cte$) is closer to what we have. (2) We have obtained European funding to do MHD simulations and we plan to investigate the role of magnetic fields in these envelopes in the near future.

KUPKA: How do you compute the length scale L in your estimates of Re ? – I think that using the total depth of the convective zone is not a very useful number, because for turbulence what matters is the energy carrying scale which is probably closer to the local pressure scale height or the width of the up- and downflows in your simulations. Thus, the effective Reynolds number is probably a lot smaller than 1000 in the red giant case and 4000 in the solar composition model.

PALACIOS: I have used the *?side, wide?* length of the computational domain.

https://doi.org/10.1017/S1743921308022722 Published online by Cambridge University Press